Experimental study of a Capillary Pumped Loop assisted with a mechanical pump placed at the evaporator inlet

Marie Lévêque, Sébastien Dutour, Jacques Lluc, Pascal Lavieille, Marc Miscevic, Yves Bertin, Raphael Mari, Laura Fourgeaud

Experimental study of a Capillary Pumped Loop assisted with a mechanical pump placed at the evaporator inlet

Marie Levêque[a,c], Sébastien Dutour[a,*], Jacques Lluc[a], Pascal Lavieille[a], Marc Miscevic[a], Yves Bertin[b], Raphael Mari[c,d], Laura Fourgeaud[c,d]

[a] *University of Toulouse, UPS, INPT, CNRS, LAPLACE, 118 route de Narbonne, F-31062 Toulouse cedex 9, France.*
[b] *Insitut Pprime CNRS-ENSMA-Université de Poitiers, ENSMA, 1 avenue Clément Ader BP 40109, F-86961 Futuroscope Chasseneuil Cedex, France*
[c] *IRT Saint-Exupéry, 3 rue Tarfaya - CS 34436, 31405 Toulouse cedex 4, France*
[d] *Airbus Defence and Space, 31 rue des Cosmonautes, 31400 Toulouse, France*

Abstract

The heat transfer performances of capillary-driven evaporators are still improving while their pumping capacity remains drastically limited by the porous wick structure. The pump assistance allows this capillary limit to be overcome and more largely, gives the opportunity of an important enhancement of capillary two-phase loops operating range. An experimental device made of a Capillary Pumped Loop coupled with a controlled centrifugal pump located at the inlet of the evaporator was proposed. We have shown that the hybrid system acts as it would in a simple capillary-driven regime with an operating loop pressure drop far beyond the capillary limit (more than 60 kPa i.e. more than 6 times the evaporator capillary limit with methanol) while preserving the evaporator thermal efficiency due to vaporisation. Moreover, we have found that the pump assistance significantly increases the system robustness during large amplitude heat load step and startup by influencing the liquid subcooling and flow rate at the evaporator inlet.

Keywords: Capillary Pumped Loop, Hybrid loop, Mechanical pumping, Electronics cooling

1. Introduction

Capillary Pumped Loop (CPL) and Loop Heat Pipe (LHP) are heat transfer and transport systems highly relevant to the cooling of electronic systems [1]. They can transfer tens of kW released at more than 100 W/cm^2 by multiple heat sources. These features are decisive in space applications and terrestrial transportation where electronic components integration is critically increasing.

The loop performance is mainly related to the capillary evaporator efficiency. The vaporisation of the working fluid within a porous wick leads to the formation of a complex liquid-vapor interface made of small menisci pumping the liquid at the pore scale. This process results in a quasi-uniform evaporator wall temperature with a high heat transfer coefficient between the evaporator wall and the fluid. Moreover, as the menisci could adjust their curvature according to the interface pressure drop, the liquid pumping at the evaporator inlet is adapted to the vaporisation rate. Thus, the evaporator thermal performance can be maintained for a large range of heat loads without any external flow control. However, the evaporator differential pressure available for pumping reaches a maximum inherent to the porous structure and fluid properties (the capillary limit). For instance, this limit is about 25 kPa for wick with 2 μm pore mean radius and with ammonia as the working fluid [2]. When the loop pressure drop exceeds this limit, the vapor deeply spreads within the wick. This can deteriorate the wick pumping leading to the evaporator dry-out and a critical temperature increase of the dissipative sources.

The LHP and CPL coupling with a mechanical pump is a way to overcome this capillary limit. More generally, it gives the opportunity of an important enhancement of the capillary two-phase loops performance. Schweickart et al. [3] studied a hybrid loop configuration consisting of a CPL assisted by a volumetric pump. The CPL included eight parallel evaporators, ten meters of both liquid and vapor lines, six parallel condenser lines, a subcooler, and a thermally controlled reservoir. The mechanical pump was placed downstream the reservoir at the inlet of the evaporators. A specific controller was developed so that the flow rate was controlled as a function of the loop heat load. Tests have demonstrated a greater heat transport capability. However, this improvement appeared to be restricted to a 14% heat load increase because of many limitations other than the evaporators pressure drop such as evaporator liquid flooding.

A different configuration of a hybrid loop with two flat-type capillary driven evaporators and a volumetric gear pump was developed by Park et al. [4], Crepinsek and Park [5], [6]. The objective was to transfer heat flux higher than 100 $W\,cm^{-2}$ such as required by power electronics cooling. A liquid loop circulation starting and finishing at the reservoir was ensured by the mechanical pump located downstream the reservoir. The liq-

*corresponding author
Email address: sebastien.dutour@laplace.univ-tlse.fr (Sébastien Dutour)

uid flowed through the liquid chambers within the evaporators but, as the porous wick of the evaporators constituted one of the wall of these liquid chambers, part of the flow was sucked within the liquid line by capillary forces when vaporisation was established in the wick. Then, the vapor returned to the reservoir by a bypass line finally leading to a parallel hybrid loop. Actually, a successful operation was shown for heat load up to $1.2\,kW$ and $102\,W\,cm^{-2}$ with a total differential pressure close to $60\,kPa$. However, liquid flooding of the evaporators was observed at low and moderate heat loads leading to a significant decrease of the thermal performance. An active control scheme adjusting the flow rate in the main liquid branch was then developed by Bejarano and Park [7]. A more stable operation was actually reached but some temperature fluctuations due to some partially flooded evaporator regimes were not totally avoided. Using a close configuration of a parallel hybrid loop, Jiang et al. [8] provided some results indicating the effect of liquid charging [9] and conducting a deep investigation of loop startup [10].

Another hybrid approach was proposed by Setyawan et al. [11] in order to prevent the LHP evaporator dry-out which may occur during the startup process at high heat load. A small diaphragm pump was placed on a bypass of the liquid line directly entering within the evaporator core. The vapor outlet temperature monitoring was used to control the power supply to the pump. In this configuration, the pressure drop was not supported by the mechanical pump and thus, the maximum pumping pressure was still imposed by the porous wick. However, the modified LHP could handle startup at $200\,W$ while the dry-out limit was reached for a start-up at $140\,W$ without the pump. This investigation demonstrated that the pump assistance of a LHP gave the opportunity to adjust the subcooling required by the wick, and then, the hybrid loop approach is also promising for some heat transfer limitation such as transient wick dry-out during the startup process.

For all hybrid configurations previously described, the control of the phase distribution in the evaporator appeared to be a critical issue. Actually, the pump assistance significantly affected the adaptation of the flow rate to the heat load of the capillary-driven evaporator so that partial liquid flooding in the wick deteriorated the evaporator conductance. Consequently, new coupling approaches have to be examined.

In this study, a CPL previously developed for power electronics cooling is assisted with a centrifugal pump located upstream the evaporator. This is a series configuration of a hybrid loop close to Schweickart et al. [3] device. One of the advantages is that the evaporator design and the CPL architecture were unchanged contrary to the parallel hybrid architecture. However, in the present work, the pump is used as a differential pressure source in the liquid line which is a different approach from [3] where the volumetric pump directly affected the liquid flow rate and the phase distribution in the evaporator. A control scheme of the rotational speed of the pump is proposed. The response to power cycle and the startup dynamics are investigated with the objective to demonstrate that the hybrid CPL (HCPL) behaves as a simple CPL system with operating pressure drop in the line far beyond the capillary limit and with preserved evaporator thermal efficiency. The leading mechanisms ruling out the HCPL performances are also discussed.

2. Experimental set-up

2.1. HCPL set-up

The HCPL consists of a vertical flat evaporator, a thermally regulated reservoir located above the evaporator and a counter-flow double pipe condenser (see figure 1). The evaporator casing has two active faces which are in contact with a rectangular sintered nickel porous wick with trapezoidal vapor grooves directly machined on the whole wick surface. The maximum evaporator pressure gain was determined at given heat load, by carefully closing the valve located on the vapor line until the evaporator deprime. A constant value of $9 - 10kPa$ was found for the heat load operating range. It is close but lower than the Laplace-Young theoretical value ($10.5\,kPa$) assuming spherical menisci with the wick mean pore diameter. This is consistent with the fact that the theoretical value gives the pressure drop accros the interface which thus includes additional pressure drop in the wick and the vapor grooves and collectors.

The condenser is a double coaxial glass tube heat exchanger connected to a thermostatted bath chiller using a transparent coolant allowing to visualize the flow patterns and dynamics. It is located about $18\,cm$ below the evaporator i.e. in an unfavorable position as the capillary force must overcome a total gravitational pressure difference of about $4\,kPa$. The reservoir configuration is such that the liquid flow between the condenser and the evaporator is maintained in the lower portion by a perforated plate. Then, a heater provides the saturation temperature regulation via a PID controller. The lines are thermally insulated. Power is uniformly applied to both sides of the evaporator. The maximum power input is imposed by the condenser design. Its value is found to be $1.6\,kW$ with a cold source at $25°C$. The main geometrical features are provided in table 1. A very close CPL configuration was previously investigated by [12] while similar evaporators were used in [13],[14].

The centrifugal pump is placed between the reservoir and the evaporator (liquid line 2). It was especially built to be entirely hermetic. The impeller is located in a sealed casing including two fluid connectors. It is driven by magnetic force.The rotational speed ranges from $4,000\,rpm$ to $30,000\,rpm$ with a maximal speed increase of $2,000\,rpm$ per second. The relation between the pump pressure gain Δp, mass flow rate $\dot{m}$ and rotational speed w is:

$$\Delta p = a\,w^2 - b\,w\,\dot{m} \tag{1}$$

where a and b are constants given in table 1.

Hence, by controlling the rotational speed, a given pressure gain can be reached for a large mass flow rate range as shown in figure 2. The maximum pressure gain is $60\,kPa$. The pump power is proportional to the rotational speed power three. The operating power is $[1.5 - 13]\,W$. The selection of the pump according to CPL specification was performed using numerical simulations of the HCPL response versus the operating conditions [15] based on the CPL modeling provides by [16].

Components	Dimensions
Evaporator	$320 \times 81 \times 20\,mm$
	wall thickness : $1\,mm$
Wick	$283 \times 68 \times 16\,mm$
	mean pore diameter : $6.8\,\mu m$
	permeability : $6.53\ 10^{-13}\ m^2$
	porosity : 73%
Vapor line	i.d. : $12\,mm$
	length : $3.3\,m$
Condenser	i.d. : $12\,mm$
	length : $7.2\,m$
Liquid line 1	i.d. : $6\,mm$
(reservoir inlet)	length : $1.5\,m$
Reservoir	volume : $2\ 10^{-3}\ m^3$
Liquid line 2	i.d. : $10\,mm$
(evaporator inlet)	length : $1\,m$
Pump	volume : $18 \times 9 \times 4\,cm$
	mass : $650\,g$
	a : $7.3\ 10^{-5}\ Pa\,(tr/min)^{-2}$
	b : $90\ Pa\,kg^{-1}\ s\,(tr/min)^{-1}$

Table 1: HCPL main features.

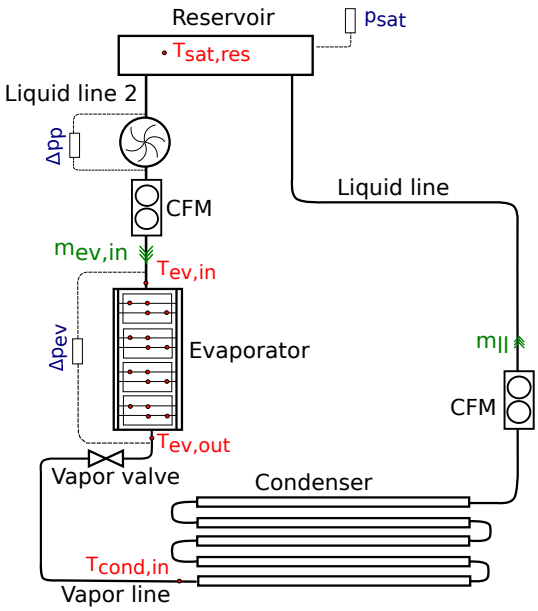

Figure 1: Schematic of the HCPL with instrumentation. CFM: Coriolis Flow Meter.

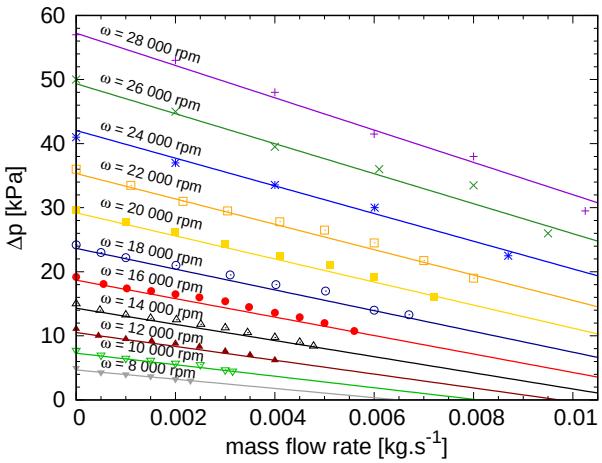

Figure 2: The pump pressure gain with methanol vs the mass flow rate and rotational speed. Points correspond to experimental results and lines to the relation (1) outcome.

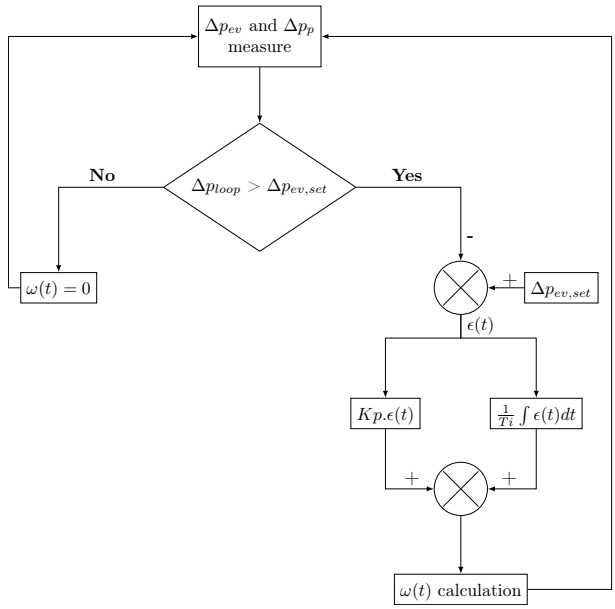

Figure 3: Simplified block diagram of the HCPL control scheme.

A schematic view of the HCPL instrumentation is also shown in figure 1. The evaporator wall temperature measurements are performed using K-type thermocouples (diameter $0.5\,mm$) inserted into small grooves of $0.6\,mm$ diameter made in the evaporator casing. Additional thermocouples are conventionally placed on the external surface of pipes along lines. After calibration, the thermocouples accuracy is $\pm 0.1\,K$. Pressure transducers are placed on the loop to measure with an accuracy of $\pm 100\,Pa$ the pressure difference between the fluid entrance and exit of the evaporator, the centrifugal pump and lines. The pressure in the saturation part of the reservoir is monitored by an absolute $0 - 2\,bar$ (accuracy : $\pm 400\,Pa$) transducer connected to the upper part of the reservoir. Combined with a $2\,mm$ diameter platinum probe placed in the vapor, the pressure measurements are also used for the in situ detection of non-condensable gases. The liquid mass flow rate at the inlet and at the outlet of the reservoir are determined with an accuracy less than $\pm 1\,\%$ using Coriolis flowmeters. Data acquisition is carried out at a frequency of $40\,Hz$ except for the flow rate which is performed every second.

In order to remove non-condensable gases, the liquid

methanol was preliminarily boiled in a separated device and high vacuum was reached in the HCPL before filling.

2.2. Evaporator differential pressure control scheme

An active pump control scheme (see figure 3) is used in order to maintain the capillary driven pumping even when the total pressure drop in the loop, Δp_{loop}, exceeds the capillary limit. The monitoring of the pressure drop in the loop is performed by measuring the differential pressure at the evaporator Δp_{EV} and at the pump Δp_p as Δp_{loop} is also given by the sum of both driving pressures :

$$\Delta p_{loop} = \Delta p_{EV} + \Delta p_p \tag{2}$$

Then, comparing this pressure drop to a set point for the evaporator pressure $\Delta p_{EV,set}$, two regimes can be achieved :

- when $\Delta p_{loop} \geq \Delta p_{EV,set}$, the mechanical pump is started and an automatic control regulates the rotational speed ω such as Δp_{EV} remains as close as possible to the set point : the HCPL reaches the pump-assisted capillary-driven (PACD) regime.
- when $\Delta p_{loop} < \Delta p_{EV,set}$, the mechanical pump is switched off and then acts as a passive component from hydraulic point of view: the HCPL operates in a simple capillary-driven (CD) regime.

A proportional-integral (PI) controller is used during the PACD regime. Values of both constants K_P and T_I were experimentally adjusted observing the system response. $\Delta p_{ev,set}$ has to be set lower than $9 - 10\,kPa$ (the maximum evaporator pressure gain) in order to prevent the evaporator dry-out and greater than $2\,kPa$ (liquid hydrostatic pressure within the evaporator) in order to prevent the liquid flooding. The value of $6\,kPa$ was chosen for all experiments.

2.3. Experimental procedure

Some important CPL performance limitations due to the capillary limit are (i) a restricted heat transport capacity, (ii) loop deprime during large amplitude heat load steps [12] and (iii) loop deprime when the startup process is achieved at high power [17]. Consequently, this study investigated the HCPL response to these sollicitations and compared it to the response obtained with the same CPL system but without pump assistance.

A control valve located in the vapor line enabled to increase the pressure losses in the loop. As a consequence, the maximum heat load before the CPL deprime could be artificially adjusted before starting the power cycle. Two different loop pressure drop operating regimes were used: a low pressure drop (LPD) regime with a fully open control valve and a high pressure drop (HPD) regime with an almost close valve plug. With a larger heat load operating range, the LPD regime was suitable in order to investigate the loop thermal performance. The HPD regime was used in order to test the system with a maximum loop pressure drop such as during the first experiments which were performed with objective to demonstrate that the HCPL improved the transport capacity. The reservoir temperature and the coolant temperature were respectively maintained to $65°C$ and $25°C$. Then, heat load steps were applied to the evaporator. A moderate step amplitude of $0.2\,kW$ was chosen in order to limit the flow inertia.

The influence of the transient when the heat load step became larger and during high power startup, was respectively performed in a second and a third series of experiments. Actually, in these operating conditions, CPL faced severe fluid dynamics and pressure drop change due to the fluid redistribution which allowed to test the robustness of the control strategy.

3. Experimental results and analysis

3.1. Heat transport capacity increase and evaporator thermal performances

Figure 4 confirms that the operating range of the CPL is drastically limited in the HPD regime. The first heat load step leads to a steady-state at $400\,W$ but the liquid subcooling at the evaporator inlet is significantly deteriorated by boiling or vapor percolation as shown by the evaporator inlet temperature increase and the inlet flow rate oscillations. The evaporator dry-out is then observable during the next heat load step from $400\,W$ to $600\,W$: at $t = 45\,min$, the evaporator differential pressure suddenly drops just after reaching the capillary limit. Simultaneously, the mass flow rate at the evaporator inlet stops until the vapor fully invades the evaporator inlet. Finally, the wall temperature drastically increases and the power has to be switched off.

Figure 5 shows the HCPL response to the same previous power cycle shown in figure 4. A large increase of the operating range is observable since the HCPL is still functioning at $1.6\,kW$. Moreover, the total HCPL differential pressure has reached up to $60\,kPa$ which corresponds to more than 6 the capillary limit and more than 4 the CPL heat transport capacity.

A more detailed analysis shows that the HCPL automatically switches from the CD to the PACD regime during the heat load step from $200\,W$ to $400\,W$ and vice versa. This demonstrated that the mechanical pump is successfully started or stopped by the control scheme. During the PACD regime, the evaporator differential pressure appears to be almost insensitive to the loop pressure drop increase while the liquid mass flow rate at the evaporator inlet is adjusting to the vaporisation rate at steady-state. Actually, the capillary evaporator is still acting as it would in a simple CPL system except that the additional loop pressure drop are taken up by the mechanical pump. Moreover the stability of the evaporator pressure highlights the efficiency of the regulation system and the suitable response time of the pump. Furthermore, the fluid temperature at the evaporator inlet shows that the pump maintains the liquid subcooling: at $400\,W$, $T_{ev,in}$ is $52°C$ while $T_{ev,in}$ is close to the vapor temperature $T_{ev,out}$ on figure 4. The pump is thus able to prevent penetration of the vapor phase within the porous wick and boiling during the step transient.

In addition, figure 6 shows that, at steady-state, there is an increase of the subcooling with the heat flux in both CPL and

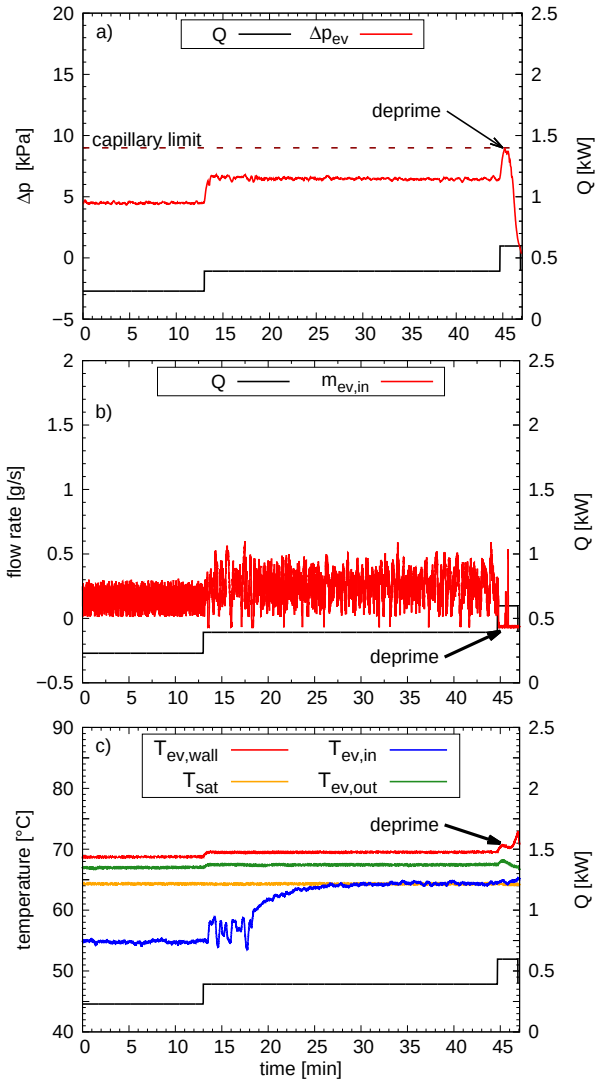

Figure 4: Example of evaporator dry-out and CPL deprime consecutive to the heat load increase in the HPD regime: evaporator differential pressure a), mass flow rates b) and temperature variation c) versus time.

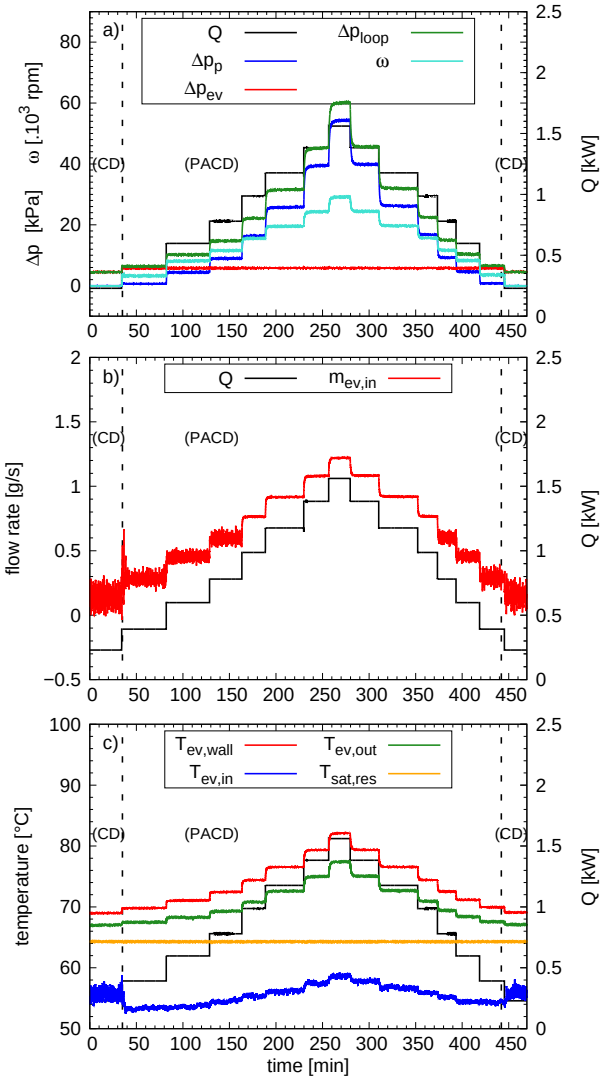

Figure 5: HCPL response to moderate heat load steps in the HPD regime: pressure differences and pump rotational speed a), mass flow rate at the evaporator inlet b) and temperature variation c).

HCPL configurations. These results were obtained in the LPD regime in order to maximize the heat load operating range. However, the subcooling becomes significantly larger at high heat load in the HCPL configuration. This is mainly due to the pressure increase at the inlet of the evaporator leading to a greater saturation temperature $T_{sat}(P_{ev,in})$ increase than the liquid temperature increase $T_{ev,in}$ due to thermal conduction. As a consequence, the HCPL also allows to move away from the boiling limit.

No significant discontinuity in the evaporator wall temperature measurements is observable between both regimes so that the thermal performance of the capillary driven evaporator seems to be unaffected by the pump assistance. Figure 7 shows the evaporator global conductance versus the heat load for both CPL and HCPL systems in the LPD regime. This conductance is a characteristic of the heat transfer including conduction through the evaporator casing and vaporisation in the porous wick. The definition is :

$$G_{ev} = \frac{\dot{Q}_v}{T_{ev,wall} - T_v} \tag{3}$$

where $T_{ev,wall}$ is the (average) external wall temperature, T_v is the temperature of the vaporisation interface and $\dot{Q}_v$ is the heat conducted to the vaporisation interface which was determined knowing the heat applied to the evaporator and the heat losses with ambient. T_v was obtained by the experimental determination of the pressure p_v in the vapor grooves assuming that T_v is the saturation temperature at p_v.

Figure 7 definitively demonstrates that the pump assistance is not leading to the evaporator flooding as there is no significant

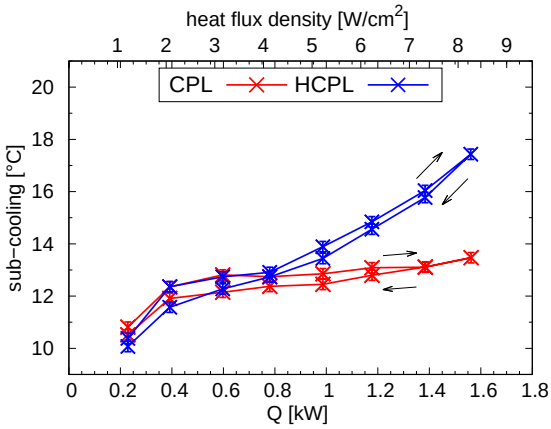

Figure 6: Liquid subcooling at the evaporator inlet versus the heat load for CPL and HCPL systems in the LPD regime.

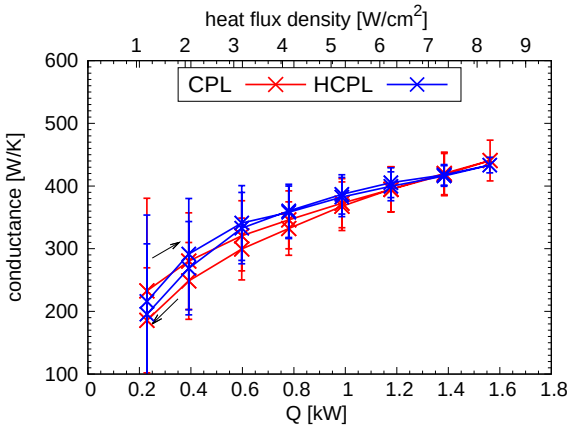

Figure 7: Evaporator conductance versus the heat load for CPL and HCPL systems in the LPD regime.

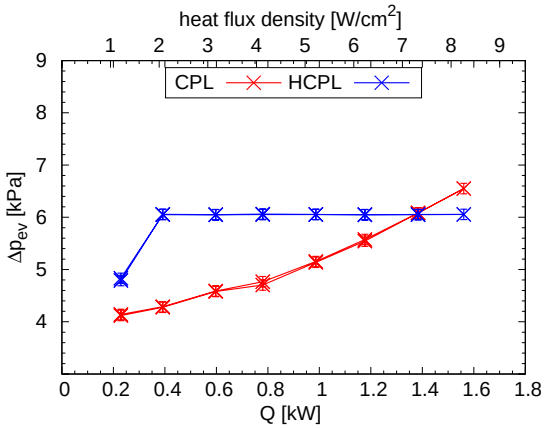

Figure 8: Evaporator differential pressure versus the heat load for CPL and HCPL systems in the LPD regime.

deviation between both conductance series in the LPD regime. We thus conclude that the HCPL system maintains the evaporator thermal performance corresponding to the vaporisation regime in the wick on the full operating range.

Beyond the performance enhancement, these results also give the opportunity to question the understanding of the heat transfer in a capillary-driven evaporator. Indeed, the HCPL allows studying the evaporator conductance versus the heat load, the evaporator pressure drop and the vapor temperature. Figure 8 shows the evaporator pressure gain corresponding to the steady-states presented on Figure 7. For the CPL, the pressure difference normally increases with the heat load while, for HCPL, the evaporator pressure gain is controlled when the loop pressure drop becomes greater than the set point. For a given heat load, the vaporisation in both tests thus occurred at different pressure drop and finally, at different vapor temperature. Both figures 7 and 8 then suggest that, for this device and within the considered operating range, the conductance is not really influenced by the pressure drop but it is mainly affected by the heat load. Here, the conductance increases with the heat load. However, at larger heat loads, Accorinti et al. [14] showed that the conductance reached a maximum and then decreased with the heat load. This is consistent with the experimental results obtained by Liao and Zhao [18] with a wick heated by a finned surface and more recently by Odagiri and Nagano [19] with heated grooves directly machinated in the porous wick.

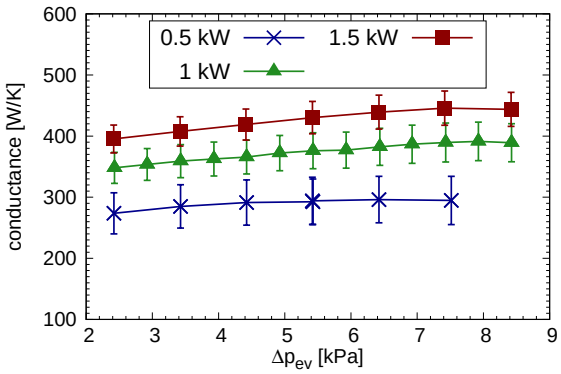

Figure 9: Evaporator conductance versus the evaporator differential pressure at fixed heat loads.

The weakly dependance of the conductance with the evaporator pressure drop is confirmed on figure 9 showing the conductance versus the evaporator pressure difference. The experiments were performed at a fixed heat load and for a given pressure drop in the loop by changing the evaporator set point $\Delta p_{EV,set}$ from 2.4 kPa to 8.5 kPa. A small conductance increase is perceptible, however, it is not really significant compared to the modification observed with the heat load.

The increase of the evaporator conductance with the heat load at low heat load is still open issue. As observed by [19], the vaporisation in the wick results of heat transfer at both the

meniscus and the porous wick scales. At very low heat load, the liquid superheat in the wick remains limited and the wick is saturated with liquid. Vaporisation takes place at the wick/groove interface. Some additional menisci could also persist between the casing and the grooves. In the case of a liquid full wick, the variation of the evaporator conductance with the heat load is introduced by the variation of the menisci curvature with the heat load i.e. a more curved meniscus leads to a thinner meniscus extension in contact to the wick resulting in heat transfer enhancement. However, with an increase of the heat load, nucleate boiling occurs in the wick. A two-phase zone is then developing within the wick as observed by [18] and [19]. In this case, the evaporator conductance increase with the heat load is given by the increase of triple line/micro-region at the wick/casing interface as shown by Mottet et al. [20] and Nishikawara et al. [21] with 3D pore-network simulations. The vapor presence at this interface is then driven by (i) the pores invasion due to the evaporator pressure difference increase, (ii) the bubble nucleation because the liquid reaches its superheat limit. Then, at larger heat load, the fraction of liquid pores in contact with the casing drastically decreases and finally a vapor pocket appears leading to a significant conductance decrease. According to these results, the conductance results plotted in figure 9 shows that the menisci curvature radius has a very small influence on the heat transfer regime in our experiments. This also suggests that, in the operating conditions, vapor and liquid should coexist in the wick, while bubbles nucleation should be the dominant process of the two-phase zone extension at the wick/casing interface resulting in the conductance increase with the heat load.

3.2. *Robustness of the control strategy during large amplitude heat load step*

Here, the evaporator dry-out is observed for the simple CPL configuration in the LPD regime when a heat load step from $0.2\,kW$ to $1.4\,kW$ is applied. Figure 10 shows the HCPL response to a step from $0.2\,kW$ to $1.6\,kW$ and thus, demonstrates that the HCPL is able to deal with larger heat load steps than a simple CPL.

A more detailed analysis indicates that, before the step, the HCPL operates in a steady-state CD regime as the pressure drop in the loop was lower than the evaporator set point. Then, the large amount of vapor consecutive to the heat load increase leads to an important mass flow rate overshoot in the liquid line (m_{ll}). As a consequence, the pressure drop in the loop significantly increases and the evaporator differential pressure reaches the capillary limit. Simultaneously, the inlet evaporator flow rate drops and penetration of the vapor phase within the wick can be detected by the increasing of the evaporator inlet temperature. The centrifugal pump starts few seconds after the heat load change and attempts to regulate the evaporator pressure drop. In this way, it limits the vapor percolation and moreover, it increases the liquid subcooling required to condensate the vapor and to re-establish by imbibition the capillary-driven regimes. With the evaporator differential pressure decrease, the rotational speed decreases and finally, the HCPL operates in a steady PACD regime. Additional tests in the HPD regime and

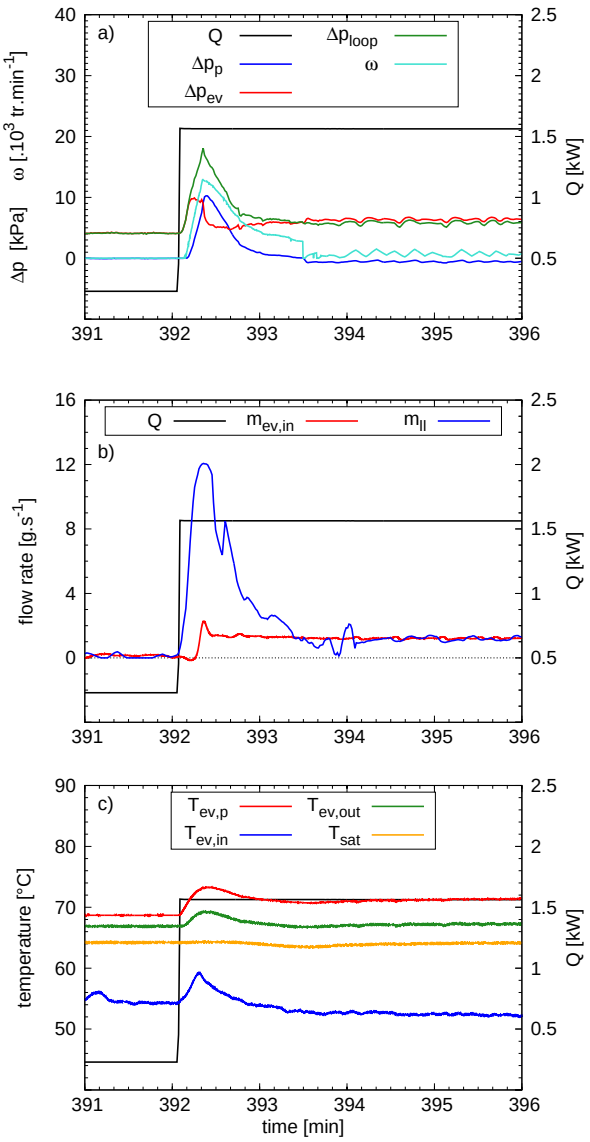

Figure 10: HCPL time response to high amplitude heat load step in the LPD regime: pressure differences and pump rotational speed a), mass flow rate at the evaporator inlet b) and temperature variation c).

step amplitude up to $2\,kW$ have confirmed the robustness of the HCPL system in handling severe heat load transients.

3.3. *Increasing the heat load at startup with pump assistance*

Figure 11 shows a startup failure when $1.1\,kW$ was applied at the evaporator in the LPD regime. As the evaporator was full of liquid, a large superheat (regime I) is achieved before nucleation occurs at $t = 2\,min\,30\,s$. Then, a large amount of vapor is suddenly produced (regime II). The pressure in the grooves largely increase and some liquid is pushed out of the evaporator by the vapor. Some vapor also percolates the wick and spreads at the inlet of the evaporator as shown by the temperature increase and a negative flow rate. This reverse flow simul-

taneously produces a large pressure drop in the pump. Here, the vapor condensation within subcooled liquid is not sufficient to re-flood the evaporator and then, the liquid supplying of the wick is stopped since $t = 2\,min\,48\,s$. Finally, the wick dry-out appears at $t = 4\,min$ as shown by the wall temperature increase and the power is shut-down. In usual conditions, the vapor at the inlet of the evaporator is condensed before the total dry-out so that the liquid supply is rapidly provided to the wick and then capillary pumping is established less than $1\,min$ after the nucleate boiling onset.

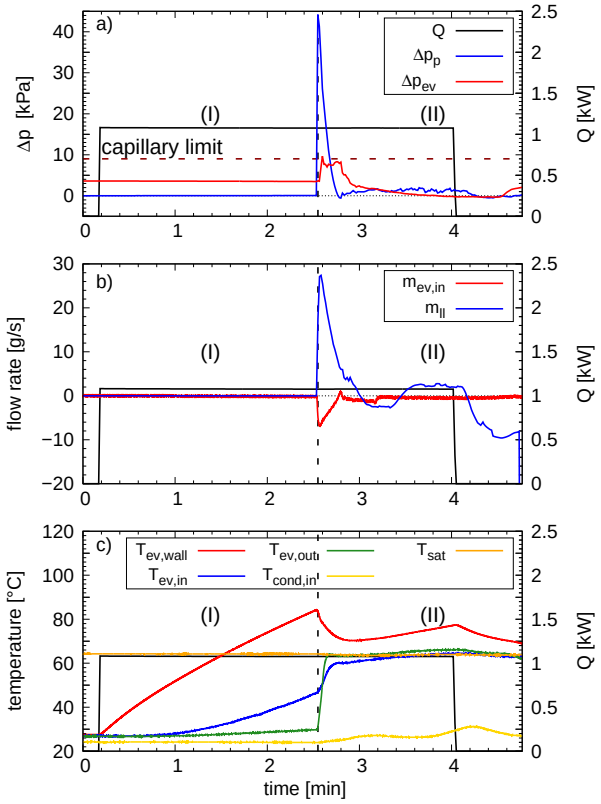

Figure 11: Example of evaporator dry-out and CPL deprime consecutive to the startup process: evaporator differential pressure a), mass flow rates b) and temperature variation c) versus time.

The HCPL startup tests were performed in the same conditions (control valve open). The control scheme was unchanged (cf. figure 3). The pump assisted system systematically succeeded. Figure 12 shows a startup performed at high heat load i.e. $1.6\,kW$. The pump automatically starts just few seconds after the onset of boiling since the evaporator differential pressure exceeds the set point ($6\,kPa$). The rotational speed of the pump ω then increases attempting to regulate the evaporator pressure drop. During this stage, the mechanical pump significantly injects some subcooled liquid from the reservoir to such an extend that at $t = 2\,min\,30\,s$ the liquid flooding of the evaporator occurs during almost $10\,s$. This is suggested by the severe decrease of the evaporator differential pressure which becomes lower than the hydrostatic value (regime I). However, the rotational speed

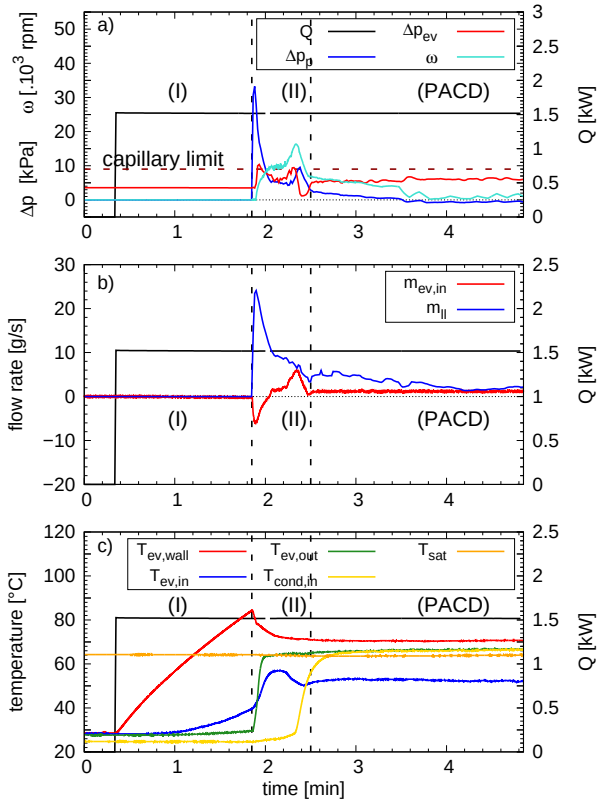

Figure 12: HCPL time response to high amplitude heat load startup: pressure differences and pump rotational speed a), mass flow rate at the evaporator inlet b) and temperature variation c).

simultaneously decreased and finally the vaporisation with capillary driven pumping and thus the PACD regime is achieved at $t = 2\,min\,42\,s$ as shown by the sudden stabilization of the liquid mass flow rate at the inlet of the evaporator. From now, the pump assistance adjusts the loop pressure drop due to the establishment of the vapor front in the condenser.

It is thus its ability to increase the liquid subcooling at the evaporator inlet when vapor transiently penetrate within the wick that explains that the pump assistance reduced the CPL startup failure at high heat loads. However, as the process variable in the control scheme is not the subcooling but the evaporator differential pressure, the HCPL could be inefficient. Actually, if HCPL is started in the HPD regime, the system startup fails as shown in Figure 13. In this test, the amount of vapor which percolates the wick is significantly larger than in the previous test as shown by a larger amplitude of the evaporator inlet reverse flow. The pump starts to regulate the evaporator differential pressure as expected but, it is not able to supply enough subcooled liquid to the evaporator before the dry-out and the power has then to be stopped at $t = 2\,min\,36\,s$. Although the HCPL failed in the latest case, an optimisation of the control scheme should provide the way to enhance the operating range of the HCPL during the startup at very high heat load.

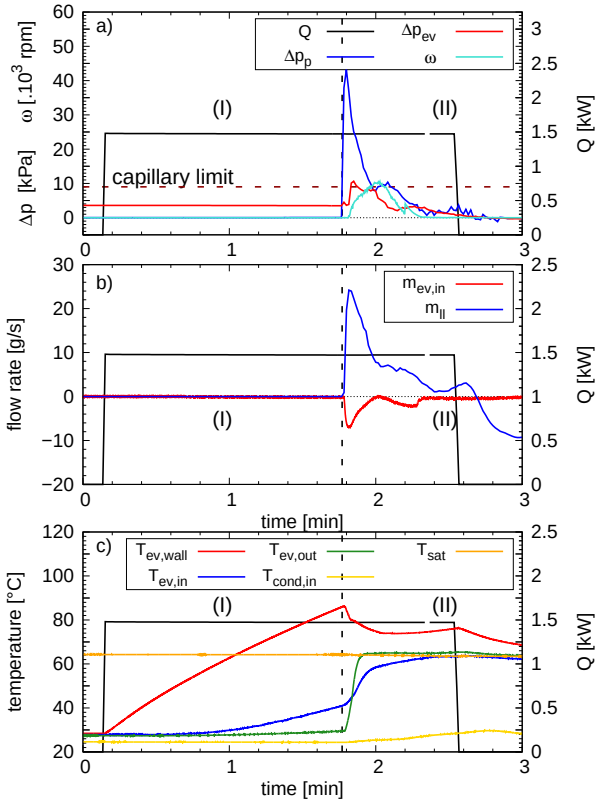

Figure 13: Example of HCPL failure consecutive to high amplitude heat load startup when large pressure drop was imposed to the loop (the vapor line valve plug was almost close): pressure differences and pump rotational speed a), mass flow rate at the evaporator inlet b) and temperature variation c).

4. Conclusion

An original hybrid loop consisting of a CPL in series with a centrifugal pump located at the evaporator inlet has been investigated. This system has shown many intrinsic advantages, since under most conditions, the operating range of a simple CPL can be significantly extended.

In particular, the experiments have demonstrated that the total loop pressure drop reached up to $60\,kPa$ during the PACD regime, corresponding to more than 6 times the evaporator capillary limit with methanol. We have simultaneously shown that the hybrid system still behaves as a simple CPL in the sense that pumping pressure and vaporisation are maintained at the evaporator so that the evaporator thermal efficiency and the internal adaptive mechanism to the heat load are fully preserved by the HCPL system. This stable behavior is quite new compared to previous hybrid devices.

Moreover, the HCPL robustness during high amplitude heat load steps and startup process have been demonstrated. By increasing the liquid pressure at the evaporator inlet, the pump assistance limits the amount of vapor which percolates the wick and increases the liquid subcooling required at the evaporator inlet to re-establish the capillary-driven regime. Although the evaporator dry-out has been reached at high heat flux and large pressure drop, the HCPL significantly increases the operating heat load range compared to the CPL configuration. An optimisation of the controller should provide the way to extend the operating range of the HCPL during the startup at very high power.

Finally, as the HCPL limit relies on the mechanical pump features, these results could mean that higher performance may be reached by using a powerful pump. Moreover, the HCPL should give the opportunity to develop capillary driven evaporators using working fluids with lower values of global warming potential even if their surface tension is weak.

Acknowledgment

Financial support from the IRT Saint-Exupéry is gratefully acknowledged.

References

[1] Y. F. Maydanik, Loop heat pipes, Applied Thermal Engineering 25 (2005) 635–657.
[2] T. Kaya, R. Pérez, C. Gregori, A. Torres, Numerical simulation of transient operation of loop heat pipes, Applied Thermal Engineering 28 (2008) 967 – 974.
[3] R. Schweickart, L. Ottenstein, B. Cullimore, C. Egan, D. Wolf, Testing of a controller for a hybrid capillary pumped loop thermal control system, IEEE 69 (1989).
[4] C. Park, A. Vallury, J. Zuo, Performance evaluation of pump-assisted capillary two-phase loop, ASME Journal of Thermal Science and Engineering Applications 1 (2009).
[5] M. Crepinsek, C. Park, Effect of Operational Conditions on Cooling Performance of Pump-Assisted Capillary-Driven Two-Phase Loop, Journal of Thermophysics and Heat Transfer 25 (2011) 572–580.
[6] M. Crepinsek, C. Park, Experimental analysis of pump-assisted and capillary-driven dual-evaporators two-phase cooling loop, Applied Thermal Engineering 38 (2012) 133–142.
[7] R. V. Bejarano, C. Park, Active flow control for cold-start performance enhancement of a pump-assisted, capillary-driven, two-phase cooling loop, International Journal of Heat and Mass Transfer 78 (2014) 408–415.
[8] C. Jiang, W. Liu, H. C. Wang, D. D. Wang, J. G. Yang, J. Y. Li, Z. C. Liu, Experimental investigation of pump-assisted capillary phase change loop, Applied Thermal Engineering 71 (2014) 581–588.
[9] C. Jiang, Z. Liu, D. Wang, J. Yang, H. Wang, J. Li, W. Liu, Effect of liquid charging process on the operational characteristics of pump-assisted capillary phase change loop, Applied Thermal Engineering 91 (2015) 953–962.
[10] C. Jiang, W. Liu, Z. Liu, J. Yang, B. Duan, X. Luo, Startup characteristics of pump-assisted capillary phase change loop, Applied Thermal Engineering 126 (2017) 1115–1125.
[11] I. Setyawan, N. Putra, I. I. Hakim, Experimental investigation of the operating characteristics of a hybrid loop heat pipe using pump assistance, Applied Thermal Engineering 130 (2018) 10–16.
[12] A. Kaled, S. Dutour, V. Platel, J. Lluc, Experimental study of a Capillary Pumped Loop for cooling power electronics: Response to high amplitude heat load steps, Applied Thermal Engineering 89 (2015) 169–179.
[13] V. Ayel, L. Lachassagne, Y. Bertin, C. Romestant, D. Lossouarn, Experimental Analysis of a Capillary Pumped Loop for Terrestrial Application, Journal of Thermophysics and Heat Transfer 25 (2011) 561–571.
[14] F. Accorinti, V. Ayel, Y. Bertin, Steady-state analysis of a Capillary Pumped Loop for Terrestrial Application with methanol and ethanol as working fluids, International Journal of Thermal Sciences 137 (2019) 571–583.
[15] M. Leveque, S. Dutour, M. Miscevic, P. Lavieille, Y. Bertin, R. Mari, A theoretical investigation of a controlled hybrid mechanical/capillary

pumped loop, 2018. 19th International Heat Pipe Conference (19th IHPC), Pisa, Italia, june 12-16, 2018.

[16] S. Dutour, A. Kaled, Analytical and numerical results for the dynamics of capillary pumped loops and loop heat pipes subjected to high amplitude heat load steps, Applied Thermal Engineering 126 (2017) 1107–1114.

[17] V. Dupont, S. Van Oost, L. Barremaecker, Increasing the CPL power at startup by using a check valve, in: Proceedings of the 16th International Heat Pipes Conference (IHPC) 2012, 2012, pp. 249–254.

[18] Q. Liao, T. Zhao, A visual study of phase-change heat transfer in a two-dimensional porous structure with a partial heating boundary, International Journal of Heat and Mass Transfer 43 (2000) 1089–1102.

[19] K. Odagiri, H. Nagano, Characteristics of phase-change heat transfer in a capillary evaporator based on microscale infrared/visible observation, International Journal of Heat and Mass Transfer 130 (2019) 938–945.

[20] L. Mottet, T. Coquard, M. Prat, International Journal of Heat and Mass Transfer Three dimensional liquid and vapour distribution in the wick of capillary evaporators, International Journal of Heat and Mass Transfer 83 (2015) 636–651.

[21] M. Nishikawara, H. Nagano, M. Prat, Numerical study on heat-transfer characteristics of loop heat pipe evaporator using three-dimensional pore network model, Applied Thermal Engineering 126 (2017) 1098–1106.